THE JOURNAL OF BIOLOGICAL CHEMISTRY VOL. 285, NO. 45, pp. 34991–34998, November 5, 2010

Identification of Protein-Protein and Protein-Ribosome Interacting Regions of the C-terminal Tail of Human Mitochondrial Inner Membrane Protein Oxa1L*[S]

Received for publication, July 12, 2010, and in revised form, August 20, 2010 Published, JBC Papers in Press, August 25, 2010, DOI 10.1074/jbc.M110.163808

Md. Emdadul Haque, Linda L. Spremulli, and Christopher J. Fecko[1]

From the Department of Chemistry, University of North Carolina, Chapel Hill, North Carolina 27599-3290

The mammalian mitochondrial inner membrane protein Oxa1L is involved in the insertion of a number of mitochondrial translation products into the inner membrane. During this process, the C-terminal tail of Oxa1L (Oxa1L-CTT) binds mitochondrial ribosomes and is believed to coordinate the synthesis and membrane insertion of the nascent chains into the membrane. The C-terminal tail of Oxa1L does not contain any Cys residues. Four variants of this protein with a specifically placed Cys residue at position 4, 39, 67, or 94 of Oxa1L-CTT have been prepared. These Cys residues have been derivatized with a fluorescent probe, tetramethylrhodamine-5-maleimide, for biophysical studies. Oxa1L-CTT forms oligomers cooperatively with a binding constant in the submicromolar range. Fluorescence anisotropy and fluorescence lifetime measurements indicate that contacts near a long helix close to position 39 of Oxa1L-CTT occur during oligomer formation. Fluorescence correlation spectroscopy measurements demonstrate that all of the Oxa1L-CTT derivatives bind to mammalian mitochondrial ribosomes. Steady-state fluorescence quenching and fluorescence lifetime data indicate that there are extensive contacts between Oxa1L-CTT and the ribosome-encompassing regions around positions 39, 67, and 94. The results of this study suggest that Oxa1L-CTT undergoes conformational changes and induced oligomer formation when it binds to the ribosome.

Mammalian mitochondria synthesize 13 hydrophobic proteins that are components of the respiratory chain complexes in the inner membrane. Protein synthesis in this organelle is performed by specialized ribosomes, which are quite distinct from the ribosomes of other translational systems. In particular, they are quite rich in protein and have truncated rRNAs (1). Because of the presence of regions of high hydrophobicity, mitochondrially synthesized proteins are thought to be integrated into the membrane during or immediately following their synthesis on mitochondrial ribosomes.

Mitochondrial ribosomes are associated with the inner membrane (2, 3), and several proteins have been implicated in the binding of these ribosomes to the membrane. The best characterized of these are members of the Oxa1 family of proteins. Oxa1 is located in the inner membrane, where it acts as a component of the machinery that mediates the insertion of certain hydrophobic proteins into the membrane. It belongs to the YidC and Alb3 family of proteins found throughout prokaryotes and eukaryotes (4, 5). The human form is designated Oxa1L. Oxa1L consists of an N-terminal section located in the mitochondrial intermembrane space, five transmembrane helices, and a C-terminal tail of ~100 amino acids exposed in the mitochondrial matrix (6).

The C-terminal tail of the yeast homolog of Oxa1L (Oxa1p) has been shown to bind mitochondrial ribosomes (6). Deletion of this region of Oxa1p severely diminishes the efficiency of membrane insertion of subunit II of cytochrome oxidase, indicating that the C-terminal tail of yeast Oxa1p plays an active role in the insertion of mitochondrial translation products into the lipid bilayer (6). Cryo-EM studies of yeast Oxa1p bound to bacterial ribosomes indicate that it interacts near the exit tunnel located on the back of the large ribosomal subunit (7).

Previous studies of the C-terminal tail of human Oxa1L (Oxa1L-CTT)[2] suggested that, in solution, the C-terminal tail exists as an equilibrium of the monomer, dimer, and tetramer forms (8). Circular dichroism studies indicated that it contains ~20% α-helical content. Despite predictions based on yeast Oxa1p, human Oxa1L-CTT does not form a coiled-coil structure. Two copies of Oxa1L-CTT bind to ribosomes with a binding constant in the range of 0.3–0.8 μM. Cross-linking studies suggested that Oxa1L-CTT contacts three proteins that have bacterial homologs (MRPL13, MRPL20, and MRPL28) and three proteins that are unique to mitochondrial ribosomes (MRPL48, MRPL49, and MRPL51). These proteins are believed to be located on the solvent side of the large ribosomal subunit (8). Despite this recent work, our understanding of the structure of human Oxa1L-CTT and its interaction with the mammalian mitochondrial ribosomes is quite limited. In this study, we have investigated the regions of Oxa1L-CTT that interact during formation of the oligomer and examined which regions of Oxa1L-CTT interact with the ribosome using static and dynamic fluorescence spectroscopy.

EXPERIMENTAL PROCEDURES

Materials—High-purity grade chemicals were purchased from Sigma or Fisher. Tetramethylrhodamine-5-maleimide

* This work was supported, in whole or in part, by National Institutes of Health Grant GM32734 (to L. L. S.).

[S] The on-line version of this article (available at http://www.jbc.org) contains supplemental "Methods," Figs. S1–S3, and Table S1.

[1] To whom correspondence should be addressed. Tel.: 919-962-0528; Fax: 919-962-2388; E-mail: cfecko@email.unc.edu.

[2] The abbreviations used are: Oxa1L-CTT, Oxa1L C-terminal tail; TCEP, tris(2-carboxyethyl)phosphine hydrochloride; FCS, fluorescence correlation spectroscopy; TCSPC, time-correlated single-photon counting; 2CFI, two-component fit improvement.

was obtained from Invitrogen. Sephadex G-15 was purchased from Sigma. Bovine mitochondria and mitochondrial ribosomes (55 S) and ribosomal subunits (28 S and 39 S) were prepared as described previously (9).

Preparation of Mutant Derivatives of Oxa1L-CTT—The cDNA clone of mature human Oxa1L was obtained from American Type Culture Collection (ATCC 10961183, IMAGE 40017377). The region encompassing the C-terminal tail was cloned, expressed, and purified as described previously (8). Four mutant derivatives were prepared in which specific residues were converted to Cys (A4C, A39C, T67C, and S94C) (shown in Fig. 1, *upper*). These derivatives were prepared using the QuikChange site-directed mutagenesis protocol (Stratagene) and forward primers CGGATTCCATGTGTACGCACTGTACTTAAAATC (for position 4), GGCTGGAAAAATTGTGAAATGACG (for position 39), GGTCCTCGACAGTGTTTTACCCAC (for position 67), and AGCAAACCAAAGTGTAAGTATCCC (for position 94). The reverse primers used were the inverse complements of the forward primers in each case. All mutations carrying Oxa1L-CTT were transformed into *Escherichia coli* DH5α, and the nucleotide sequences of the inserted DNAs were confirmed. The variants are designated Oxa4-CTT, Oxa39-CTT, Oxa67-CTT, and Oxa94-CTT, indicating the position of the Cys residue. The mutant plasmids were subsequently transformed into *E. coli* BL21(DE3) RIL cells (Stratagene) for expression. Cells were grown to an A_{600} of 0.6 in LB medium containing 100 μg/ml ampicillin and 34 μg/ml chloramphenicol and induced by the addition of 50 μM isopropyl 1-thio-β-D-galactopyranoside for 6 h at 37 °C. After induction, cells were lysed, and Oxa1L-CTT was purified using nickel-nitrilotriacetic acid resin, followed by HPLC purification on a TSKgel SP-5PW cation exchange column as described previously (8) except that buffers contained 1 mM tris(2-carboxyethyl)phosphine hydrochloride (TCEP) as the reducing agent unless indicated otherwise. Proteins were purified with and without TCEP, keeping all other conditions the same. The mutant derivatives were tested for structural integrity by comparing the α-helical content obtained using circular dichroism with that of wild-type Oxa1L-CTT. The secondary structures of the Oxa1L-CTT variants did not change upon mutation at any of these positions.

Detection of Dimers by S–S Bond Formation—Oxa1L-CTT variants prepared in the absence of TCEP (5 μg, 10 μl) were kept under slow passing O_2 gas for 30 min and then held at 4 °C overnight in buffer containing 20 mM HEPES-KOH (pH 7.6) and 50 mM KCl in the presence and absence of 10 mM $MgCl_2$. An equal volume of 2× SDS loading dye without β-mercaptoethanol was added to the reaction mixtures. Samples were run on a 15% SDS-polyacrylamide gel. The gel was stained with Coomassie Blue, and the monomer and dimer bands were quantified using UN-SCAN-IT gel software.

Fluorescence Tagging of the Oxa1L-CTT Derivatives with Rhodamine—Each HPLC-purified Oxa1L-CTT variant (78 μM in 500 μl, 1 mg/ml) was labeled with rhodamine-5-maleimide basically as described by the manufacturer, producing Oxa4-Rh, Oxa39-Rh, Oxa67-Rh, and Oxa94-Rh. The concentrated fluorescent probe (33 mM dissolved in Me_2SO) was added to the protein solution in buffer containing 20 mM HEPES-KOH (pH 7.6), 50 mM KCl, and 1 mM TCEP at a molar ratio of 5:1 (probe/protein). The mixture (500-μl final volume) was incubated for 1 h at room temperature with gentle shaking in the dark. The reactions were quenched by the addition of excess β-mercaptoethanol (100 mM). Tagged proteins were separated from free dye by chromatography on a Sephadex G-15 column (0.7 × 20 cm) equilibrated in buffer containing 20 mM HEPES-KOH (pH 7.6), 50 mM KCl, 10 mM $MgCl_2$, 10% glycerol, and 1 mM TCEP. The protein concentration was calculated using the following formula: protein concentration (M) = $(A_{280} - A_{max}\cdot CF)/\epsilon$, where A_{max} is the absorbance of rhodamine-5-maleimide at the wavelength maximum (550 nm), CF is the correction factor ($CF = A_{280(free\ dye)}/A_{550(free\ dye)}$), and ϵ is the molar extinction coefficient of Oxa1L-CTT based on the amino acid composition (12,700 $M^{-1}\ cm^{-1}$). The CF value is equal to 0.34 (Thermo Scientific). The degree of labeling was calculated using the following formula: % label = A_{max} of the labeled protein/ϵ'·protein concentration, where ϵ' is the molar extinction coefficient of the fluorescent dye (65,000 $M^{-1}\ cm^{-1}$). The tagging efficiency was 70–100%.

Measurement of Rhodamine Steady-state Fluorescence Intensity and Anisotropy to Detect the Oligomer-forming Segments of Oxa1L-CTT and Binding to Ribosomes—The rhodamine fluorescence anisotropy of Oxa4-Rh, Oxa39-Rh, Oxa67-Rh, and Oxa94-Rh was examined on an SLM 48000 spectrofluorometer (SLM Aminco, Urbana, IL) using an excitation wavelength of 545 nm and an emission wavelength of 573 nm. The rhodamine-tagged protein (100 nM) was in 20 mM HEPES-KOH (pH 7.6), 50 mM KCl, 5 mM $MgCl_2$, and 1 mM TCEP. Data were collected in L-format using 0.4-cm path length quartz cuvettes with 5-nm excitation and 5-nm emission slits at 25 °C in the absence and presence of the indicated concentrations of wild-type Oxa1L-CTT. Control measurements using the corresponding buffer containing wild-type Oxa1L-CTT were recorded and subtracted from the sample readings. The fluorescence anisotropy was calculated using the following equation: $r = (I_{vv} - G\cdot I_{vh})/(I_{vv} + 2G\cdot I_{vh})$, where I_{vv} is the polarized emission intensity with vertical excitation and vertical emission polarizers, I_{vh} is the polarized emission intensity with vertical excitation and horizontal emission polarizers, and G is the instrumental correction factor (G-factor = $I_{hv}/I_{hh,}$ where I_{hh} is the polarized emission intensity with horizontal excitation and horizontal emission polarizers). For Oxa-Rh binding to ribosomes, rhodamine fluorescence intensity was recorded with the addition of ribosomes, keeping the same conditions as described above. Background intensity (ribosome alone in buffer) was monitored and subtracted from the sample reading.

Measurement of Protein Dynamics Using Fluorescence Correlation Spectroscopy (FCS) and Time-correlated Single-photon Counting (TCSPC)—FCS and TCSPC measurements were performed using a home-built, two-photon optical microscope (10, 11). This instrument uses ultrashort pulses generated by a Coherent Chameleon Ultra II laser (~140-fs pulse duration, 80-MHz repetition rate), which is tuned to 825 nm for optimal excitation of rhodamine. The laser output is attenuated by a low-bandwidth electro-optic modulator and is then directed through a second higher bandwidth electro-optic modulator that permits individual pulse selection (both modulator sys-

tems from Conoptics Inc., Danbury, CT). Residual visible light is removed by a long-wave pass filter (HQ690LP, Chroma, Rockingham, VT) before the laser beam enters an Olympus IX-81 inverted microscope through laser port B. It is focused into the sample by a 60× 1.2-numerical aperture water immersion objective; the back aperture of this lens is slightly overfilled to create a diffraction-limited focal spot. Epifluorescence collected by the objective is separated from the excitation beam by a long-pass dichroic filter (670DCXXRU, Chroma). Full suppression of the IR light and of the emission from a minor impurity in the ribosomal samples is accomplished with a short-pass dichroic filter (FF01-680/SP, Semrock, Rochester, NY) and a band pass filter (HQ630/100m-2P, Chroma). The optically filtered fluorescence is detected by a GaAsP photomultiplier tube (H7422P-40mod, Hamamatsu), the output of which is sent to a custom-designed preamplifier that has both a high-bandwidth amplified output channel and a discriminated digital output channel.

FCS measurements are accomplished by sending the digital preamplifier output to an external correlator (Flex03LQ-12, Correlator.com). These experiments were performed at the full 80-MHz pulse repetition rate, and the excitation power at the sample was typically 5–6 milliwatts. Experiments performed at lower powers resulted in identical correlation curves. The correlation curves were fit to the models described under supplemental "Methods" using a least-squares algorithm in MATLAB.

For TCSPC measurements, the pulse repetition rate was reduced to 5 MHz by the high-bandwidth modulator, and samples were excited with pulse energies of ~3 nJ. A polarizer set at the magic angle was inserted into the fluorescence path to eliminate signal contributions from molecular reorientation. Additionally, a coverslip placed in the laser beam path was used to direct a small fraction of the excitation light to a fast photodiode for use as a timing reference. To record TCSPC curves, the photodiode output and the high-bandwidth output of the photomultiplier tube preamplifier were sent to a single-photon counting module (SPC-130, Becker & Hickl). The instrument response function (full width at half-maximum ~ 260 ps) was measured by collecting the second harmonic signal generated by potassium phosphate crystals placed at the sample position. Fluorescence decay curves were fit using a least-squares algorithm in MATLAB by convolving a single-exponential or biexponential decay with the instrument response function.

RESULTS

Oxa1L-CTT is a matrix-exposed domain that binds to mitochondrial ribosomes and plays a role in the insertion of mitochondrially synthesized proteins into the inner membrane. There is no direct structural information on this protein. However, a three-dimensional model has been developed using Rosetta (8). In this model (Fig. 1), Oxa1L-CTT contains a long α-helical segment along with several shorter helical regions (Fig. 1). Four mutants were prepared to place Cys residues at specific positions of Oxa1L-CTT. The first mutation converted Ala^{4} to Cys (the numbers refer to amino acid residues in the C-terminal tail, which encompasses residues 334–436 of the full-length protein) and was expected to be positioned close to

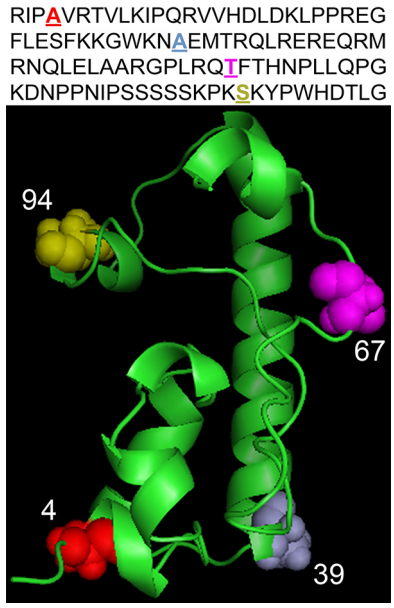

FIGURE 1. *Upper*, the primary sequence of the Oxa1L-CTT, with different colors indicating the positions where Cys was used to replace the given amino acids. The expressed protein has a methionine at the start of the sequence and LE-His_6 at the C terminus from the vector (not shown in the sequence). *Lower*, computer-generated three-dimensional structure of Oxa1L-CTT developed using Rosetta (26) and displayed using PyMOL. The Cys residues incorporated at the indicated positions are shown space-filled and in different colors.

the membrane. The second mutation converted Ala^{39} to Cys and was located at the base of the long helical segment. The third mutation (Thr^{67} to Cys) was in a loop region predicted to lie close to the long helix. Finally, the fourth mutation (Ser^{94} to Cys) was found close to the C terminus (Fig. 1). CD results indicated that the secondary structures of all Oxa1L-CTT derivatives were the same as that of wild-type Oxa1L-CTT under several buffer conditions, including the presence and absence of Mg^{2+}, indicating that the secondary structures of the variants are the same as that of the wild-type protein.

Oxa1L-CTT forms oligomers, predominantly dimers, in solution (8). To assess the regions of Oxa1L-CTT that might be in close contact in the dimer, S–S bond formation in the unlabeled proteins was forced by passing O_2 through a solution of each derivative, followed by SDS-PAGE analysis to separate monomers and dimers. The amount of dimer formed with each derivative was quantified by measuring the band intensity. In the presence of $MgCl_2$, almost 100% of Oxa39 was converted to a dimer, whereas Oxa4, Oxa67, and Oxa95 formed 25, 60, and 65% dimers, respectively (Fig. 2). The easy formation of a disulfide bond at position 39 of Oxa1L-CTT suggests that this region of the protein is in contact in the dimer. Other regions have a lower tendency to form dimers, suggesting less direct contact between them in the dimer. In the absence of $MgCl_2$, significantly different results were observed, with Oxa94 forming the most dimers and a decrease in dimer formation at position 39. There was a limited change at positions 4 and 67 in the absence of Mg^{2+}. The different patterns obtained in the presence and absence of Mg^{2+} indicate that this cation induces local conformational changes in Oxa1L-CTT. The effect of Mg^{2+} could arise from the binding of this cation to acidic residues in Oxa1L-CTT, such as the RERE sequence in the long helical

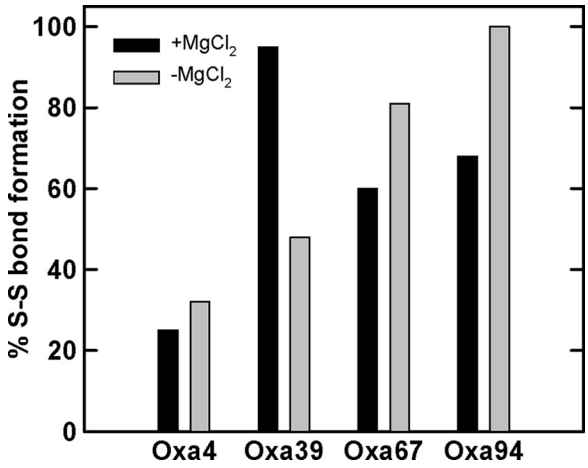

FIGURE 2. **Efficiency of disulfide bond formation of Oxa1L-CTT mutants.** Samples were treated as described under "Experimental Procedures" and analyzed by SDS-PAGE. Bands were quantified using UN-SCAN-IT gel software and are plotted as the percent S–S with respect to different mutants.

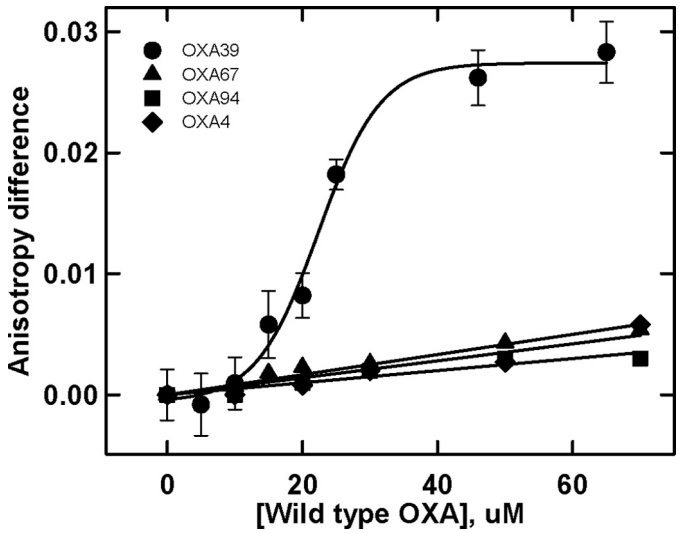

FIGURE 3. **Detection of regions of Oxa1L-CTT in close proximity using steady-state fluorescence anisotropy measurements.** Proteins tagged with rhodamine were examined using fluorescence anisotropy in the absence and presence of wild-type Oxa1L-CTT. The data are plotted as the change in anisotropy ($A_{\text{Oxa-Rh}+\text{wild-type Oxa}} - A_{\text{Oxa-Rh}}$) as a function of wild-type Oxa1L-CTT concentration. The rhodamine-labeled protein concentration was 100 nM, and the experimental details are described under "Experimental Procedures."

segment with position 39. Another possibility is the interaction of Mg^{2+} with the Glu residues at positions 26 and 30, perhaps stabilizing the short helical segment in which these residues are present.

Mitochondrial protein synthesis requires Mg^{2+}, suggesting that results obtained with Mg^{2+} are the more physiologically relevant. The concentration of monovalent salt (50–300 mM KCl) and the pH (5.5–8.5) had no effect on S–S bond formation (data not shown).

Identification of the Interacting Regions in the Oxa1L-CTT Oligomer during Formation Using Fluorescence Anisotropy Measurements—The disulfide cross-linking results suggested that the residues near position 39 are in contact in the dimer. However, random S–S bonds can form even from monomeric proteins due to random collisions. To obtain further insights into interactions that could occur in the dimer, the Cys residues in each mutant protein were derivatized with rhodamine, leading to Oxa4-Rh, Oxa39-Rh, Oxa67-Rh, and Oxa94-Rh, respectively. Each of these proteins could be fluorescently tagged with a stoichiometry of 0.7–1.0. The labeled mutants were then tested for oligomer formation using fluorescence anisotropy. Rhodamine-labeled proteins have previously been used to study protein-protein, protein-ribosome, and protein-membrane interactions (12–15).

The ability of Oxa1L-CTT to form homo-oligomers was measured by monitoring the change in fluorescence anisotropy of the Oxa-Rh derivatives by adding increasing concentrations of unlabeled (wild-type) Oxa1L-CTT (Fig. 3). There was essentially no change in anisotropy for the Oxa1L-CTT derivatives at positions 4, 67, and 94. The anisotropy of Oxa39-Rh showed little change with the addition of wild-type Oxa1L-CTT up to 10 μM but then increased with increasing concentrations until a maximum value was reached. This result clearly indicates that the segmental motion of rhodamine at position 39 is hindered (restricted rotation) in the presence of wild-type Oxa1-CTT due to oligomerization. The data for Oxa39-Rh were fit to a sigmoidal curve, indicating that Oxa1L-CTT forms homo-oligomers (dimers and tetramers) with cooperative binding. Previous work has indicated that Oxa1L-CTT exists as monomers, dimers, and tetramers in solution (8). The EC_{50} value (midpoint of the curve) and slope do not have much physical meaning in the context of our monomer-dimer-tetramer association but support an adequate description of the transition from monomer to oligomer as a function of total protein concentration. Salt (KCl) and rhodamine-tagged protein concentration data also suggest that the region around position 39 is involved mainly in oligomer formation (supplemental Fig. S1, *A* and *B*). In addition to the anisotropy change in Oxa39-Rh, the intensity of the fluorescence also decreased (by ~35%) with increasing salt and elevated protein concentrations (data not shown). Neither the intensity not the anisotropy of the other three derivatives changed under these conditions. This result indicates that with increasing Oxa1L concentrations and salt, rhodamine probes at position 39 come close together and self-quench, leading to a decrease in intensity and anisotropy (16, 17).

Microenvironment of Oxa1L-CTT Variants in Solution—We further investigated the local environment of rhodamine in each labeled position of Oxa1L-CTT by measuring the time-dependent fluorescence of each derivative under a variety of conditions. Fig. 4*a* compares the fluorescence decay of free rhodamine with that of Oxa1L-CTT labeled with rhodamine at positions 4 and 94 (each at 100 nM). The fluorescence lifetime clearly changed when rhodamine was attached to the protein, and it depended on the attachment position. Previous studies (18, 19) have found that the fluorescence lifetime of rhodamine B, which is structurally similar to the tetramethylrhodamine derivative used to label Oxa1L-CTT, varies greatly according to the solvent in which it is dissolved. Its lifetime is roughly correlated with the solvent polarity: 1.7 ns in water, 2.5 ns in methanol, 2.9 ns in ethanol, and 3.3 ns in isopropyl alcohol. On the basis of this information, we assume that the fluorescence lifetime of rhodamine is a good indicator of its local environment. When the samples in Fig. 4*a* were fit to a single-exponential

decay, the fluorescence lifetimes were 1.61, 2.38, and 3.18 ns for free rhodamine, Oxa4-Rh, and Oxa94-Rh, respectively (Table 1). It is not surprising that the local environment of rhodamine attached to the protein is less polar than in solution, but the lifetime data further indicate that rhodamine attached in position 94 is in a significantly less polar environment than rhodamine in position 4. The fluorescence lifetimes of the other Oxa1L-CTT derivatives at 100 nM indicate that the environment of rhodamine in position 39 is similar to that in position 4, whereas rhodamine in position 67 experiences an intermediate polarity. The steady-state anisotropy values were consistent with these results (0.1 for Oxa4-Rh and Oxa39-Rh, 0.147 for Oxa67-Rh, and 0.156 for Oxa94-Rh).

Interaction of Oxa1L-CTT with Ribosomes and Identification of Interacting Regions—It has been shown previously that Oxa1L-CTT binds to ribosomes with a K_d of 0.3–0.8 μM and that two Oxa1L-CTTs bind to one ribosome (8). We used two-photon excited FCS to test the ability of the Cys mutants of Oxa1L-CTT to bind ribosomes. FCS measures time-dependent fluctuations in the amount of fluorescence arising from a spatially limited observation volume within a sample (10, 11). Such fluctuations are most typically due to fluorophore diffusion through the observation volume; in this case, the characteristic time scale over which the fluorescence autocorrelation function decays (referred to as the correlation time) is inversely related to the rate of molecular diffusion. Thus, FCS can detect the association of molecules in solution by observing changes in their diffusion and is particularly useful for studying the association of large species with smaller fluorescent molecules.

Normalized fluorescence correlation functions of rhodamine, rhodamine-labeled Oxa1L-CTT derivatives alone, and rhodamine-labeled Oxa1L-CTT derivatives in the presence of ribosomes are plotted in Fig. 5. The correlation time of each of the rhodamine-labeled Oxa1L-CTT derivatives was longer than that of free rhodamine due to the increased molecular size. The correlation functions of rhodamine and all of the free protein derivatives could be fit by a model for a single diffusing species (see supplemental "Methods").

The curves for each protein in the presence of ribosomes contain a pronounced shoulder at longer lag times. These data can be fit using a two-component model in which the correlation time of the more quickly diffusing species matches that of the free Oxa1L-CTT derivative; we attribute the slowly diffusing species to the bound protein-ribosome complexes. All of the rhodamine-labeled Oxa1L-CTT derivatives bound ribosomes similarly. We performed control experiments to demonstrate that the background fluorescence in the ribosomal samples was insignificant and that free rhodamine did not interact with the ribosome or wild-type Oxa1L-CTT.

The FCS results clearly indicate that the fluorescently tagged Oxa1L-CTT derivatives are all active in binding mitochondrial ribosomes. However, these data cannot provide information on which part of the protein contacts the ribosome or on how the two Oxa1L-CTT oligomers are organized upon ribosome binding. To obtain a more detailed picture of these interactions, we measured the fluorescence intensity and fluorescence lifetime of the rhodamine-labeled Oxa1L-CTT derivatives in the absence and presence of ribosomes.

The self-quenching behavior of rhodamine was used to examine regions of the two Oxa1L-CTT monomers that are in

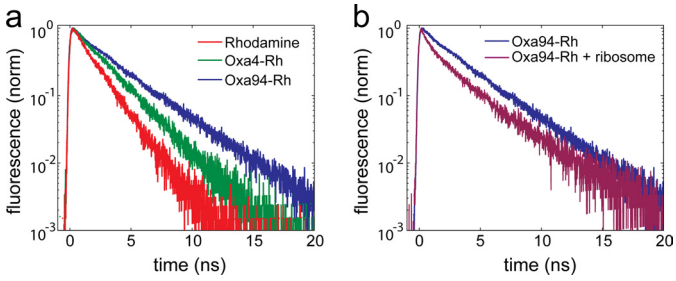

FIGURE 4. **Time-dependent fluorescence of rhodamine-labeled Oxa1L-CTT mutants as an indication of the local environment in various regions of the protein.** Samples were excited using two-photon absorption, and emission was detected at the magic angle to remove anisotropic contributions. *a*, normalized (*norm*) time-dependent fluorescence decays of free rhodamine B, Oxa4-Rh, and Oxa94-Rh. The other derivatives were omitted for clarity. *b*, comparison of Oxa94-Rh in the absence and presence of ribosomes. The protein concentration was 100 nM, and the ribosome concentration was 200 nM.

TABLE 1

Time-dependent fluorescence optimized fitting parameters

Each time-dependent fluorescence decay curve was fit to both a one-component (a·exp($-t/\tau$)) model and a two-component ($a_1$exp($-t/\tau_1$) + $a_2$exp($-t/\tau_2$)) model. The models were compared by calculating the 2CFI as the fractional decrease in the residual sum of squares for the biexponential fit expressed as a percentage, as defined under "Results." The two-component fit was used for samples that exhibited 2CFI values larger than 35%, but otherwise a one-component fit was considered adequate. Optimized fitting parameters of the most appropriate model for each sample are listed; values are the mean ± S.D. for three to five datasets. The amplitude of each fitting function was normalized; only the value of a_1 is listed for the two-component fit because $a_1 + a_2 = 1$.

	2CFI value	One-component fit (τ)	Two-Component fit		
			a_1	τ_1	τ_2
	%	ns		ns	ns
Rhodamine (100 nM)	3	1.61 ± 0.06			
Rhodamine (500 nM)	29	1.61 ± 0.04			
Oxa4-Rh (100 nM)	1	2.38 ± 0.16			
Oxa4-Rh (500 nM)	18	2.37 ± 0.03			
Oxa4-Rh + ribosome	28	2.50 ± 0.22			
Oxa39-Rh (100 nM)	34	2.35 ± 0.14			
Oxa39-Rh (500 nM)	83		0.25 ± 0.09	0.51 ± 0.10	2.46 ± 0.20
Oxa39-Rh + ribosome	189		0.44 ± 0.03	0.82 ± 0.16	2.89 ± 0.20
Oxa67-Rh (100 nM)	17	2.65 ± 0.10			
Oxa67-Rh (500 nM)	29	2.64 ± 0.36			
Oxa67-Rh + ribosome	125		0.40 ± 0.05	1.00 ± 0.25	3.06 ± 0.20
Oxa94-Rh (100 nM)	8	3.18 ± 0.13			
Oxa94-Rh (500 nM)	31	2.97 ± 0.38			
Oxa94-Rh + ribosome	158		0.50 ± 0.07	0.76 ± 0.25	3.42 ± 0.22

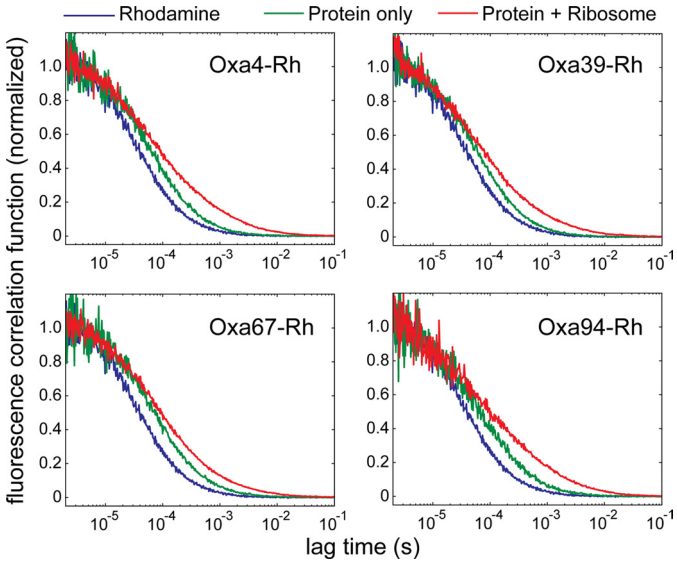

FIGURE 5. **Binding of rhodamine-labeled Oxa1L-CTT mutants to ribosomes using two-photon excited FCS.** Shown are normalized autocorrelation curves of rhodamine (*blue*), Oxa1L-CTT derivatives alone (*green*), and Oxa1L-CTT derivatives in the presence of ribosomes (*red*). FCS curves for rhodamine and the protein-only samples were fit to a one-component model; samples containing protein and ribosomes were fit to a two-component model. The protein concentration was 100 nM, and the ribosome concentration was 200 nM. Supplemental "Methods" contains more information about the models, best fit curves, and optimized fitting parameters.

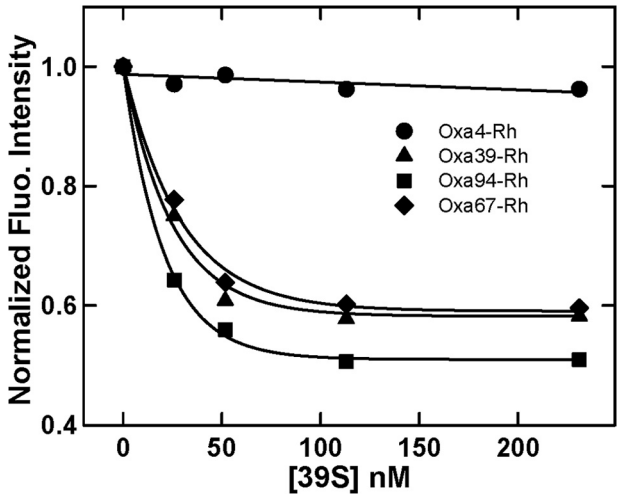

FIGURE 6. **Interaction of Oxa1L-CTT derivatives with ribosomes using rhodamine fluorescence intensity quenching.** The fluorescence (*Fluo.*) intensity of rhodamine-labeled Oxa1L-CTT mutants (100 nM) was measured in buffer and in the presence of different concentrations of ribosomes, and the normalized intensity is plotted as a function of the ribosome concentration.

close proximity when bound to the ribosome. As indicated in Fig. 6, very little decrease in fluorescence intensity (self-quenching) was observed with Oxa4-Rh, indicating that this region of the protein is not in close proximity when Oxa1L-CTT is bound to the ribosome. However, changes in fluorescence intensity were observed with Oxa1L-CTT labeled at position 39, 67, or 94. This observation indicates that the rhodamine probes at these positions have come closer together. Of these three positions, only position 39 appeared to be close in Oxa1L-CTT when the dimer (oligomer) was formed in solution. This close proximity is reflected in the interaction of the two copies of Oxa1L-CTT bound to the ribosome as observed

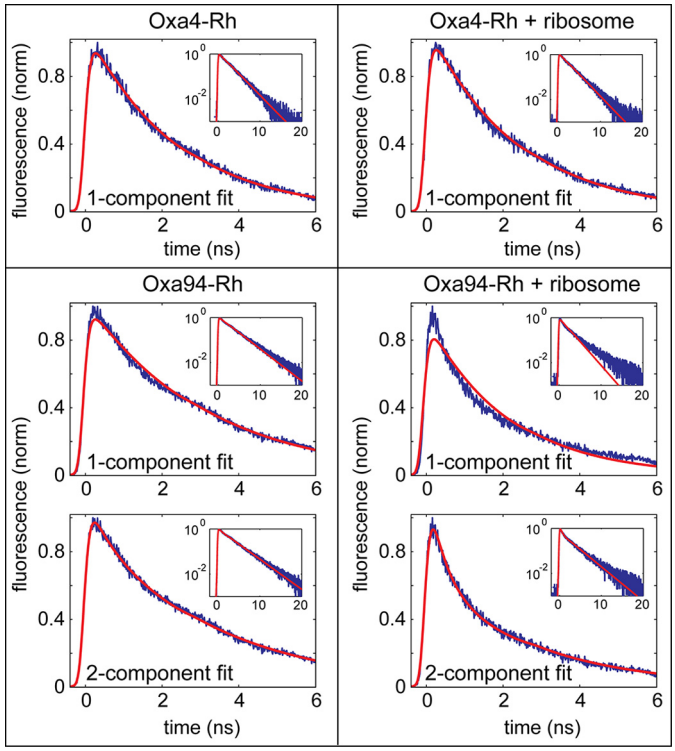

FIGURE 7. **Data-fitting strategy for time-dependent fluorescence decays of rhodamine-labeled Oxa1L-CTT mutants.** Each dataset was separately fit to a one-component (single-exponential) model and to a two-component (biexponential) model. The residual sum of squares for the two models was compared to determine the most appropriate model for each sample, as described under "Results" and in Table 1. *Upper left*, Oxa4-Rh (500 nM) fit by a single-exponential model. *Upper right*, Oxa4-Rh (100 nM) + ribosome (200 nM) fit by a single-exponential model. *Lower left*, Oxa94-Rh (500 nM) fit by a single-exponential model and a biexponential model. Both fits track the data reasonably well, but the single model was deemed adequate according to the criteria outlined under "Results." *Lower right*, Oxa94-Rh (100 nM) + ribosome (200 nM) fit to a single-exponential and a biexponential model. The biexponential model is required to adequately fit the data.

previously (8). Furthermore, these data indicate that the regions of the protein near positions 67 and 94, which were not close together in the dimer in solution, underwent conformational changes upon the binding of Oxa1L-CTT to the ribosome, bringing them into close proximity. The data were fit using a simple binding model; the apparent K_d is ~25 nM. The K_d in this study is lower than the value obtained with isothermal titration calorimetry and surface plasmon resonance used in a previous study (8). The difference in the K_d could be due to differences in the percentage of active ribosomes in various preparations or to inactivation of a portion of the ribosomes in some of the previous measurements.

With the exception of Oxa4-Rh, in the presence of ribosomes, the time-dependent fluorescence of the rhodamine-labeled Oxa1L-CTT derivatives did not adhere to a single-exponential decay (Table 1). This behavior is exemplified by comparing Oxa94-Rh in the absence and presence of ribosomes (Fig. 4*b*). It is clear that a biexponential decay model is required to fit the latter data; however, the choice between a single-exponential and a biexponential model is not as apparent for some samples (Fig. 7). To obtain a quantitative comparison of the two models, we used the residual sum of squares that resulted from a single-exponential and a biexponential fit of each decay curve.

We defined the two-component fit improvement (2CFI) as the fractional decrease in the residual sum of squares (RSS) for the biexponential fit expressed as a percentage: $2CFI = 100 \cdot ((RSS_{2\text{-component}} - RSS_{1\text{-component}})/RSS_{2\text{-component}})$. Because of experimental noise, the biexponential model improved the fit for nearly all experimentally measured decay curves ($2CFI > 0$), so we further required a threshold value to use in assigning the most appropriate model for each decay curve. Because free rhodamine is expected to exhibit single-exponential fluorescence decay kinetics at submicromolar concentrations, we set the threshold at the 2CFI value of the 500 nM rhodamine sample. A two-component fit was used for samples that exhibited improvements significantly larger than free rhodamine, but otherwise a one-component fit was considered adequate.

Table 1 lists the 2CFI values and the optimized fitting parameters of the most appropriate model for each sample. At a sufficiently low concentration (100 nM), all four rhodamine-labeled Oxa1L-CTT derivatives were adequately fit by a single-exponential model. The 2CFI values for the 500 nM samples indicate that the fluorescence decay of rhodamine at positions 4, 67, and 94 is single-exponential, whereas rhodamine at position 39 requires a biexponential fit. The longer time constant for the Oxa39-Rh variant at 500 nM matches the corresponding time constant to 100 nM within experimental error. We attribute the shorter biexponential time constant to quenching upon oligomer formation at the higher concentrations. These data are consistent with the disulfide cross-linking and fluorescence anisotropy results indicating that position 39 is in closest contact when Oxa1L forms dimers in solution, as discussed above.

The FCS results demonstrate that all four Oxa1L-CTT variants bound ribosomes, but under the same conditions, TCSPC shows that the fluorescence of rhodamine at position 4 was unaffected, whereas rhodamine at positions 39, 67, and 94 was significantly quenched. These data also confirm the steady-state quenching presented in Fig. 6. They are consistent with the model in which Oxa1L-CTT binds to ribosomes as a dimer (or oligomer) because rhodamine at position 39 was quenched at higher concentrations in the protein-only samples. Rhodamine at positions 67 and 94 exhibited more quenching than expected based on the protein-only data, which could be due to a conformational change upon binding. Therefore, we conclude from the lifetime and steady-state fluorescence data that Oxa1L-CTT binds to ribosomes as an oligomer and may undergo a conformational change.

DISCUSSION

Oxa1L plays an important role in the insertion of proteins into the inner membrane of mitochondria through an interaction of the matrix-localized C-terminal tail with the large ribosomal subunit. Fig. 8 shows the schematic model for the organization of Oxa1L in the membrane and when it binds to ribosomes. Our results indicate that human Oxa1L-CTT can dimerize and that the formation of the dimer depends on contacts around position 39 of the tail. Additional contacts are likely to occur in the transmembrane helices (20). The interaction near position 39 remains strong as the two Oxa1L-CTT monomers bind to the ribosome. However, there are substantial conformational changes in other regions of the C-terminal tail when the protein binds to ribosomes, affecting especially regions close to residues 67 and 94 (Fig. 8). These interactions indicate a significant rearrangement of residues in the tail during the formation of the functional Oxa1L-ribosome interaction. The data also indicate that there is no detectable interaction between the ribosome and regions of Oxa1L-CTT near position 4. This residue is near the portion of the C-terminal tail that emerges from the membrane, suggesting that contacts between the ribosome and Oxa1L are mediated by residues that may be spatially separated from direct contact with the membrane.

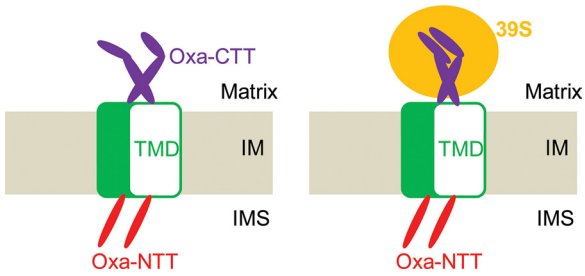

FIGURE 8. **Schematic model of Oxa1L organization in the membrane and when it binds to ribosomes.** In the absence of ribosomes, Oxa1L probably exists as a dimer with the main interacting regions in the transmembrane segments and around position 39 in the C-terminal tail. When Oxa1L binds to ribosomes, it undergoes a conformational change, and positions 67 and 94 come into close contact. *NTT*, N-terminal tail in the intermembrane space (*IMS*); *TMD*, transmembrane domain in the inner membrane (*IM*); *CTT*, C-terminal domain in the matrix.

This work represents the first application of FCS and TCSPC to the study of the binding of a ligand to mitochondrial ribosomes. FCS and TCSPC have previously been used widely for monitoring biological events (21–25). For example, FCS was used to study ligand binding to *E. coli* ribosomes (23) and to monitor both *in vivo* and *in vitro* translation (24). In this work, the use of static and dynamic fluorescence spectroscopy has allowed us to monitor the segmental interactions within protein molecules and to map the interacting regions between Oxa1L-CTT and mammalian mitochondrial ribosomes. We have specifically introduced the use of tetramethylrhodamine labeling and TCSPC as a means to assess the local polarity in various regions of a protein by correlating the fluorescence lifetime enhancement with solvent-dependent lifetime data. This approach could be applied to investigate the surface environment of other proteins. Finally, the combination of FCS and fluorescence quenching was essential to confirm the association of labeled proteins with mitochondrial ribosomes in solution and to provide spatial information about their interaction. FCS is ideally suited to monitor the binding of individual proteins to relatively massive ribosomes, and therefore, it could become a valuable tool to study the interaction of other ligands with ribosomes.

Acknowledgment—We thank Kevin Elmore for help with protein expression and purification.

REFERENCES

1. O'Brien, T. W., Denslow, N. D., Faunce, W., Anders, J., Liu, J., and O'Brien, B. (1993) in *The Translational Apparatus: Structure, Function Regulation*

and Evolution (Nierhaus, K., Franceschi, F., Subramanian, A., Erdmann, V., and Wittmann-Liebold, B., eds) pp. 575–586, Plenum Press, New York
2. Liu, M., and Spremulli, L. L. (2000) *J. Biol. Chem.* **275,** 29400–29406
3. Bonnefoy, N., Fiumera, H. L., Dujardin, G., and Fox, T. D. (2009) *Biochim. Biophys. Acta* **1793,** 60–70
4. Luirink, J., Samuelsson, T., and de Gier, J. W. (2001) *FEBS Lett.* **501,** 1–5
5. Ott, M., and Herrmann, J. M. (2010) *Biochim. Biophys. Acta* **1803,** 767–775
6. Szyrach, G., Ott, M., Bonnefoy, N., Neupert, W., and Herrmann, J. M. (2003) *EMBO J.* **22,** 6448–6457
7. Kohler, R., Boehringer, D., Greber, B., Bingel-Erlenmeyer, R., Collinson, I., Schaffitzel, C., and Ban, N. (2009) *Mol. Cell* **34,** 344–353
8. Haque, M. E., Elmore, K. B., Tripathy, A., Koc, H., Koc, E. C., and Spremulli, L. L. (2010) *J. Biol. Chem.* **285,** 28353–28362
9. Matthews, D. E., Hessler, R. A., Denslow, N. D., Edwards, J. S., and O'Brien, T. W. (1982) *J. Biol. Chem.* **257,** 8788–8794
10. Magde, D., Elson, E., and Webb, W. (1972) *Phys. Rev. Lett.* **29,** 705–708
11. Hess, S. T., Huang, S., Heikal, A. A., and Webb, W. W. (2002) *Biochemistry* **41,** 697–705
12. Hamman, B. D., Oleinikov, A. V., Jokhadze, G. G., Bochkariov, D. E., Traut, R. R., and Jameson, D. M. (1996) *J. Biol. Chem.* **271,** 7568–7573
13. Maag, D., and Lorsch, J. R. (2003) *J. Mol. Biol.* **330,** 917–924
14. Banerjee, A., Hu, J., and Goss, D. J. (2006) *Biochemistry* **45,** 2333–2338
15. Forouhar, F., Huang, W. N., Liu, J. H., Chien, K. Y., Wu, W. G., and Hsiao, C. D. (2003) *J. Biol. Chem.* **278,** 21980–21988
16. Kao, P. H., Lin, S. R., and Chang, L. S. (2007) *Toxicon* **50,** 952–959
17. MacDonald, R. I. (1990) *J. Biol. Chem.* **265,** 13533–13539
18. Magde, D., Rojas, G. E., and Seybold, P. G. (1999) *Photochem. Photobiol.* **70,** 737–744
19. Casey, K. G., and Quitevis, E. L. (2010) *J. Phys. Chem.* **92,** 6590–6594
20. Sato, T., and Mihara, K. (2009) *J. Biol. Chem.* **284,** 14819–14827
21. Haupts, U., Maiti, S., Schwille, P., and Webb, W. W. (1998) *Proc. Natl. Acad. Sci. U.S.A.* **95,** 13573–13578
22. Sherman, E., Itkin, A., Kuttner, Y. Y., Rhoades, E., Amir, D., Haas, E., and Haran, G. (2008) *Biophys. J* **94,** 4819–4827
23. Jermutus, L., Kolly, R., Földes-Papp, Z., Hanes, J., Rigler, R., and Plückthun, A. (2002) *Eur. Biophys. J.* **31,** 179–184
24. Nomura, Y., Tanaka, H., Poellinger, L., Higashino, F., and Kinjo, M. (2001) *Cytometry* **44,** 1–6
25. Jia, Y., Sytnik, A., Li, L., Vladimirov, S., Cooperman, B. S., and Hochstrasser, R. M. (1997) *Proc. Natl. Acad. Sci. U.S.A.* **94,** 7932–7936
26. Bradley, P., Misura, K. M., and Baker, D. (2005) *Science* **309,** 1868–1871